Hindawi
Active and Passive Electronic Components
Volume 2018, Article ID 7628598, 7 pages
https://doi.org/10.1155/2018/7628598

Research Article

Multitransmission Zero Dual-Band Bandpass Filter Using Nonresonating Node for 5G Millimetre-Wave Application

Liyun Shi [1,2] **and Jianjun Gao** [1]

[1] *School of Information and Science Technology, East China Normal University, 500 South Lianhua Road, Shanghai, China*
[2] *School of Electronic Information and Electronical Engineering, Shanghai Jiao Tong University, 800 Dongchuan Road, Shanghai, China*

Correspondence should be addressed to Liyun Shi; shiliyun525@163.com

Received 14 May 2018; Revised 11 November 2018; Accepted 29 November 2018; Published 13 December 2018

Academic Editor: S. M. Rezaul Hasan

A planer millimetre-wave dual-band bandpass filter with multitransmission zeros is proposed for 5G application. This filter includes two dual-mode open-loop resonators. The U-shape nonresonating node is employed to generate an extra coupling path. Finally, a dual-band bandpass filter with five transmission zeros is obtained. The filter is fabricated and measured. Good agreement between simulation and measurement is obtained.

1. Introduction

The fifth-generation mobile communication system (5G) is currently experiencing rapid development. The Third-Generation Partnership Project's (3GPP) Release-16, or "5G phase 2", should be completed in December 2019 [1]. There are three typical usage scenarios for 5G, including Enhanced Mobile Broadband (eMBB), Massive Machine Type Communications (mTC), and Ultrareliable and Low-Latency Communications (uRLLC), which were defined by the International Telecommunication Union-Radio Communication Sector (ITU-R) in 2015. To achieve very high-speed data transmission, the 5G high-frequency systems will have much wider operating bands as well as multiband. As a key passive circuit block in these systems, bandpass filters (BPFs) featuring multiband, high out-of-band power rejection and miniaturization are very attractive [2]. These BPFs efficiently reject out-of-system interferences while preserving processed signals in-band, where a specific narrow frequency band needs to be strongly attenuated. Much effort has been devoted to designing 5G millimetre-wave BPFs with high selectivity, compact size, and low cost, as shown in [2–9]. In [3–5], substrate integrated waveguide (SIW) technology is applied to design millimetre-wave BPFs. SIW technology has the advantage of a high Q-factor and easy integration with other planar circuits. In [6], a magic-T with imbedded Chebyshev filter response is developed with a multilayer, low-temperature cofired ceramic (LTCC) technology, which is popular due to its low dielectric loss, high material reliability and compatibility, and high level of robustness. However, its application is limited by the thick substrate's large feature size. In recent years, with the rapid scaling down of advanced complementary metal-oxide semiconductor (CMOS) technology, many on-chip millimetre-wave BPFs have been implemented in CMOS technology as shown in [7–9], which could provide good performance but have high cost and difficult fabrication. Compared with the above technologies, printed circuit technology still has advantages for millimetre filter design as the mainstream technology at low frequency, such as its low profile, easy fabrication, and easy integration with other planer circuits.

Bandpass filters with multiband and high selectivity are attractive because they could meet the demand for multiband wireless communication systems. Usually, filtering selectivity could be generally enhanced by producing transmission zeros (TZs) at finite real frequencies [10]. Several methods have been reported to introduce transmission zeros. In [10] an original and simple method of signal-interference source/load coupling is employed to improve filters' selectivity. In [11], special coupling topology is designed to introduce electromagnetic coupling between nonadjacent resonators. An SIW filter with etched capacitive slots at the coupling

region is proposed in [12]. These slots could create a negative coupling coefficient but also result in a higher radiation loss.

The nonresonating node concept has recently been applied to synthesize high selectivity single-band planar filters as discussed in [13, 14]. In [14], a stepped-impedance nonresonating node is employed to introduce an extra signal transmission path between the source and the load. The underlying idea is to use these elements to generate alternative interresonator couplings favouring transmission zero creation. In this paper, the realization of high selective dual-band millimetre-wave BPF by means of nonresonating node is approached. Additionally, two dual-mode open-loop resonators are employed in this filter. Dual-mode open-loop resonators are well known for their compact size and have been used for bandpass filter design in [15–17], which only use a single type of resonator and show good performance. Hence, the dual-mode open-loop bandpass filters in millimetre-wave applications are worthy of study.

The aim of this paper is the presentation of a millimetre-wave filter design that achieves a very good trade-off between performance and fabrication cost. The organization of the rest of the manuscript is as follows: Section 2 expounds on the theoretical foundations of dual-band bandpass filters. Nonresonating nodes are analyzed and discussed in Section 3. Finally, the conclusions of this study are described in Section 4.

2. Design of the Dual-Band BPF

Figure 1 shows the detailed configuration of the proposed filter. In fact, this filter can be seen as a constitution of five resonators. Two dual-mode open-loop resonators are denoted by L_1, L_2, L_3, L_4, W_1, and W_3. The nonresonating node is denoted by L_7, L_8, and W_4, which produces extra coupling paths. Compared with traditional feedlines, two 1/4 wavelength resonators are added to the CPW feedlines.

Dual-mode open-loop resonators are well known for their compact size, which is much smaller than the conventional dual-mode loop resonator [15–17]. Dual-mode open-loop filters can excite two nondegenerate modes as well as two controllable finite-frequency transmission zeros, which can be controlled simply by varying the size of perturbation.

Figure 2 shows the simulated resonant frequency response which is plotted for different values of L_2 and W_2. As can be seen from Figure 2(a), when L_2 and W_2 are changed the even mode resonant frequency is effectively shifted, while the odd mode resonant frequency is much less affected. It is also interesting to notice from Figure 2(b) that there are two finite-frequency transmission zeros when the two modes split. One transmission (TZ_1) is allocated on the left side of the passband, while the other (TZ_2) experiences a significant frequency shifting.

Since the dual-mode resonator is composed of symmetric structures, even-odd mode theory can be adopted to analyze its equivalent circuit structure and its equivalent circuit is given in Figure 3. For even mode excitation, the symmetry plane along the dashed line AA′ is considered as an open end which can be seen from Figure 3(a). The resonator works like

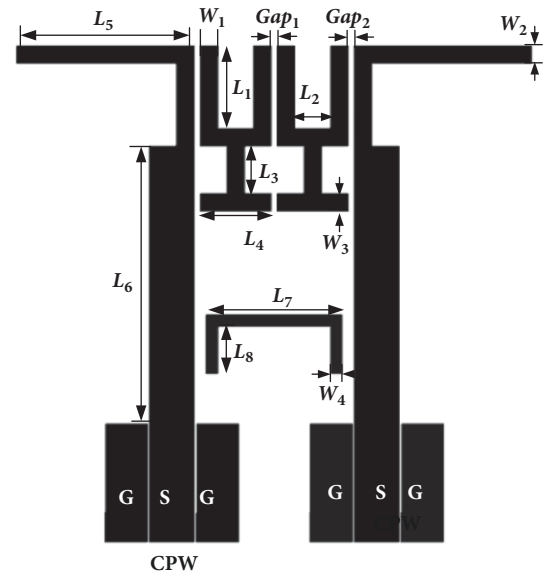

Figure 1: Schematic views of the proposed dual-band BPF.

a stepped impendence resonator (SIR) at even mode resonant frequency. The resonant condition can be calculated by (1)-(7):

$$Y_{even} = Y_{up,even} + Y_{low,even} \tag{1}$$

$$Y_{low,even} = \frac{j\tan(\theta_1 f_{e1})}{Z_1} \tag{2}$$

$$Y_{up,even} = \frac{(Q_a - Q_b)}{(P_a - P_b)} \tag{3}$$

where

$$P_a = Z_1 Z_2^2 Z_3 - Z_1 Z_2^3 \tan(\theta_3 f_e)\tan(\theta_4 f_e) \tag{4}$$

$$P_b = -Z_1^2 Z_2 \tan(\theta_2 f_e)\tan(\theta_4 f_e) - Z_3 \tan(\theta_2 f_e)\tan(\theta_3 f_e) \tag{5}$$

$$Q_a = jZ_1 Z_2 \tan(\theta_4 f_e) + jZ_1 Z_3 \tan(\theta_2 f_e) \tag{6}$$

$$Q_b = jZ_2^2 \tan(\theta_3 f_e)\tan(\theta_4 f_e)\tan(\theta_2 f_e) \tag{7}$$

For odd mode excitation, its equivalent circuit is shown in Figure 3(b). The resonator works like a uniform impedance resonator (UIR) at the odd mode resonance frequency. The resonant condition can be described by

$$Y_{odd} = \frac{j(\tan(\theta_1 f_0)\tan(\theta_2 f_0) - 1)}{Z_1} \tag{8}$$

where $\theta_1 = \beta(L_1 + L_3)$, $\theta_2 = \beta(L_2/2)$, $\theta_3 = \beta L_3$, $\theta_4 = \beta L_4$, θ_i, β, Zi are the electrical length, phase constant, and characteristics impedance of resonator, respectively, $f_e = f_{even}/f_r$, $f_o = f_{odd}/f_r$, f_{even}, f_{odd}, f_r present the even mode resonate frequency, odd mode resonate frequency, respectively.

The frequency of two transmission zeros can be obtained when input admittance at even mode or odd mode is zero. It is

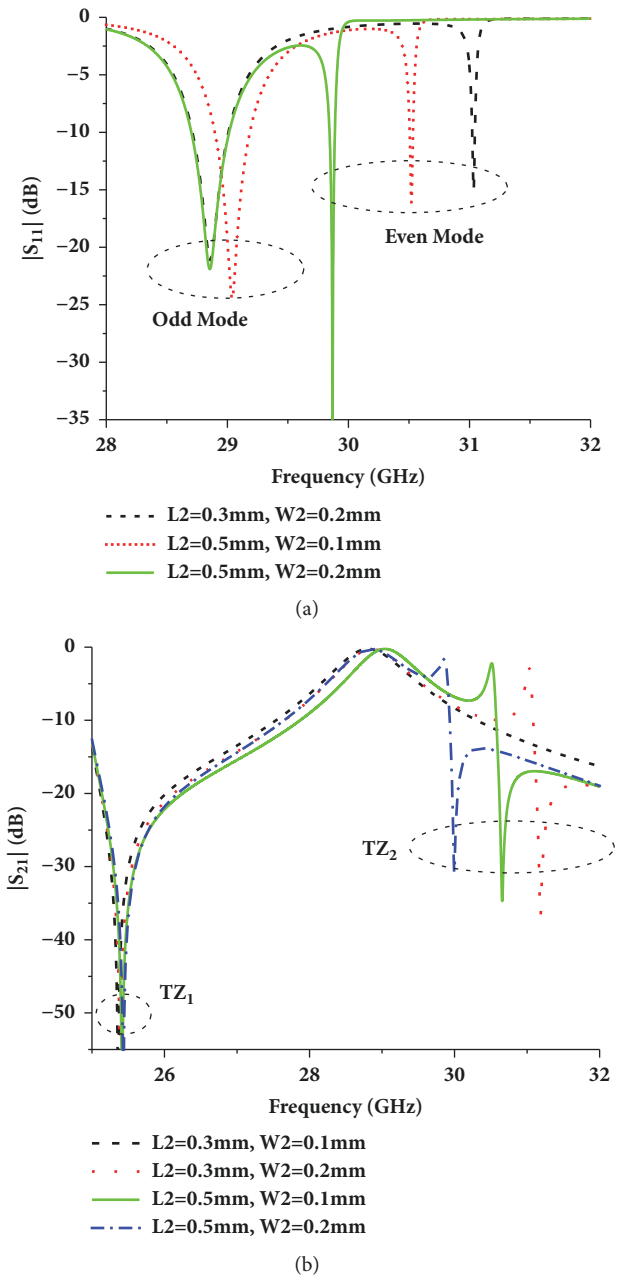

FIGURE 2: Simulated frequency responses of the dual-mode open-loop resonator with different size of L_2 and W_2 (mm): (a) S_{11} responses; (b) S_{21} responses.

noted that both f_{odd} and f_{even} can be estimated approximately by the half-wavelength of this microstrip resonator. They are obtained by (9)-(10):

$$f_{even} = \frac{2c}{(L_1 + L_3 + L_2/2 + L_4/2)\sqrt{\varepsilon_{eff}}} \quad (9)$$

$$f_{odd} = \frac{4c}{(L_1 + L_2/2)\sqrt{\varepsilon_{eff}}} \quad (10)$$

where ε_{eff} is the effective relative permittivity of substrate.

3. Analysis of Nonresonating Node

Nonresonating nodes have been employed to generate transmission zeros because they could provide multiple signal-interaction paths [18, 19]. To explain the nonresonating nodes, an original method based on a low-pass prototype with a nonresonating node is described. Elements of the low-pass prototype nonresonating node are given by the method in [19, 20], to yield a response with prescribed transmissions.

The coupling scheme of a second-order filter with no transmission zero in the cascaded configuration is shown in Figure 4(a). The dark nodes are resonators and the

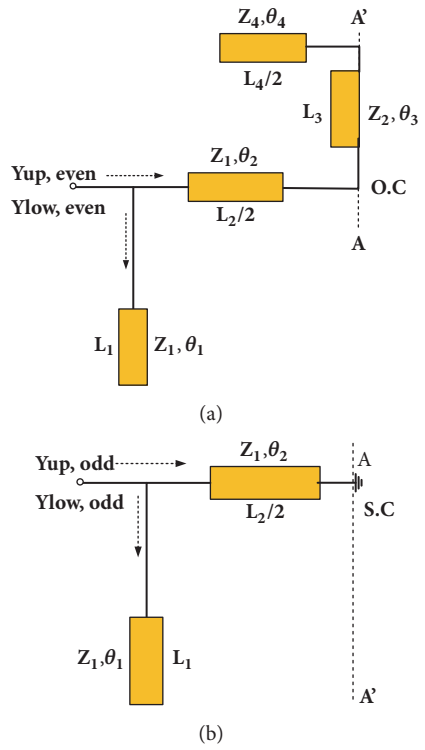

Figure 3: Equivalent circuit of different modes: (a) even mode; (b) odd mode.

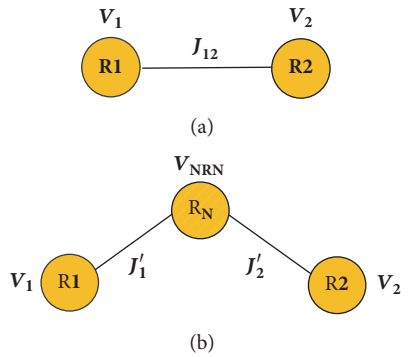

Figure 4: (a) First coupling scheme of two-order filter with none transmission zeros; (b) second coupling scheme of two-order filter in-line configuration with nonresonating nodes (patterned circles).

lines connecting them are admittance inverters. A second-order loss-pass prototype which realizes the same response is shown in Figure 4(b). Note the presence of additional nonresonating nodes, shown as the patterned circles in this prototype.

For the two cells in Figure 4 to be equivalent, they must have the same node equations (admittance matrix) or the same normal modes. The node matrix equation of the cell in Figure 4(a) is shown in

$$\begin{bmatrix} \omega + J_{11} & J_{12} \\ J_{12} & \omega + J_{22} \end{bmatrix} \begin{bmatrix} V_1 \\ V_2 \end{bmatrix} = \begin{bmatrix} e_1 \\ e_2 \end{bmatrix} \tag{11}$$

where ω is the normalized frequency, VI and V2 are the node voltages, and e1 and e2 are the excitations at the same nodes. The normalized frequency shifts of the resonators are J_{11} and J_{22}, respectively. On the other hand, the node matrix equation of the cell in Figure 4(b) is given by

$$\begin{bmatrix} \omega + b_1' & 0 & J_1' \\ 0 & \omega + b_2' & J_2' \\ J_1' & J_2' & J_{NRN} \end{bmatrix} \begin{bmatrix} V_1 \\ V_2 \\ V_{NRN} \end{bmatrix} = \begin{bmatrix} e_1 \\ e_2 \\ 0 \end{bmatrix} \tag{12}$$

where V_{NRN} is the voltage of the internal nonresonating node which is not externally excited. The normalized frequency shifts of the resonators are b1′ and b2′, respectively. The susceptance of the NRN is JNRN. If the voltage VNRR is

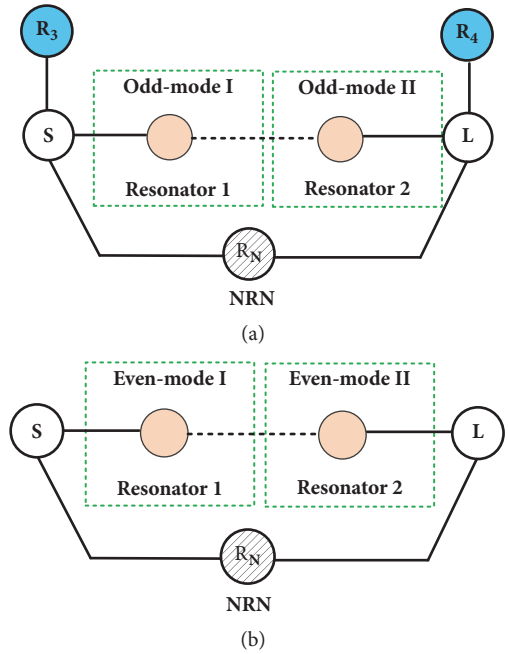

Figure 5: Coupling structure of the proposed dual-band bandpass filter. (a) At lower passband. (b) At upper passband.

eliminated from (12), by using the last row, we get the new matrix equation:

$$\begin{bmatrix} \omega + b_1' - \dfrac{J_1'^2}{J_N} & -\dfrac{J_1'}{J_N} \\ -\dfrac{J_1' J_2'}{J_N} & \omega + b_2' - \dfrac{J_2'^2}{J_N} \end{bmatrix} \begin{bmatrix} V_1 \\ V_2 \end{bmatrix} = \begin{bmatrix} e_1 \\ e_2 \end{bmatrix} \tag{13}$$

By directly comparing (11) and (13), we get the elements of the coupling matrix of the cascaded cell in Figure 4(a) in terms of the elements of the cell with an internal nonresonating node in Figure 4(b), described by (14)-(16).

$$J_{11} = b_1' - \frac{J_1'^2}{J_N} \tag{14}$$

$$J_{22} = b_2' - \frac{J_2'^2}{J_N} \tag{15}$$

$$J_{12} = -\frac{J_1'^2}{J_N} \tag{16}$$

In our design, one U-shaped nonresonating node is employed to increase source-load coupling paths. The coupling and routing scheme in the inset of Figure 4 can be used to model the configuration of the proposed filter. The coupling structure for the designed dual-band bandpass filters is shown in Figure 5, where resonators 1 and 2 denote two dual-mode open-loop resonators and resonators 3 and 4 denote L-shape feedline resonators. The white circles are source and load; blue circles are resonating nodes; the patterned circle is a nonresonating node; solid lines are main direct couplings; dashed lines are minor cross couplings. Figure 5(a) illustrates the schemes at a lower resonant frequency and Figure 5(b) is at an upper resonant frequency. Note that Figure 5 gives the main coupling structure; some other very small couplings could also take place in the proposed filter schemes.

Indeed, this nonresonating node is a resonator at certain frequencies in a strict sense; it works as a detuned folded open-ended transmission-line resonator in our design. This particular geometry could help to create a pair of transmissions zeros on both sides of the passband. As seen from Figure 2, the odd mode resonant frequency is located at the lower passband, and the even mode resonant frequency is at the higher passband. Additionally, the two L-shaped feedlines (described by L_5 and W_2) work as two resonators and their resonant frequencies are also at the lower passband. To demonstrate this design concept, a filter without a nonresonating-node is also simulated. Note that the only difference between the two filters is whether there is a nonresonating-node; the rest of the parameters are the same. Performance comparisons are illustrated in Figure 6. It is clear that two extra transmissions zeros are produced with a nonresonating node.

4. Results and Discussion

Based on the above discussion, one dual-band millimetre-wave bandpass filter has been manufactured and measured. The filter is fabricated on substrate Rogers 5880 with permittivity of 2.2, loss tangent of 0.001, and thickness of 0.254 mm, which could suppress the occurrence of high-order modes and the substrate surface-waves. The dimensions of this dual-band filter indicated in Figure 1 are L_1=1.4 mm L_2=0.6 mm, L_3=0.8 mm, L_4=1.2 mm, L_5=3 mm, L_6=6.7 mm, L_8=0.8 mm, W_1 =W_2= W_3 =0.3 mm, and W_4=0.2 mm. The width of this

Table 1: Performance comparison between the proposed design and some previously published millimetre-wave filters.

Ref.	Passband (GHz)	Insertion Loss (dB)	Fabrication Technology	Number of TZs	Size (mm^2)
[1]	28	0.4	waveguide	2	5,600,000
[2]	28	2.2	SIW	2	93.7s65
[5]	24	4.5	LTCC	1	59.625
[7]	28	2.6	CMOS	2	0.038
This work	28.1/31.1	2.1/2.5	PCB	5	72

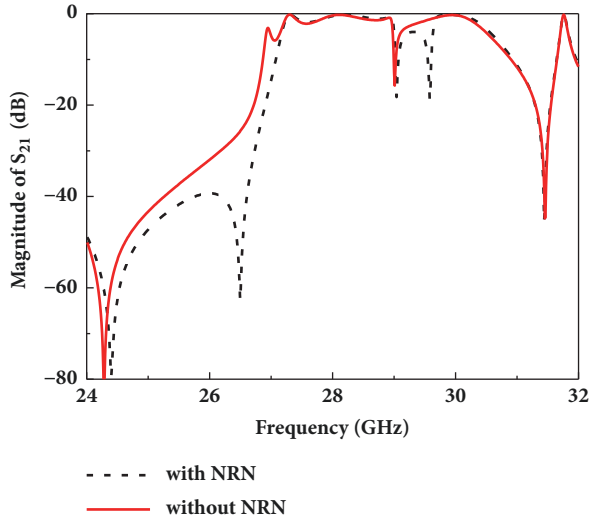

Figure 6: Comparisons of simulated S21 of the proposed BPF (solid line: filter without nonresonating node; dash line: filter with measured nonresonating node).

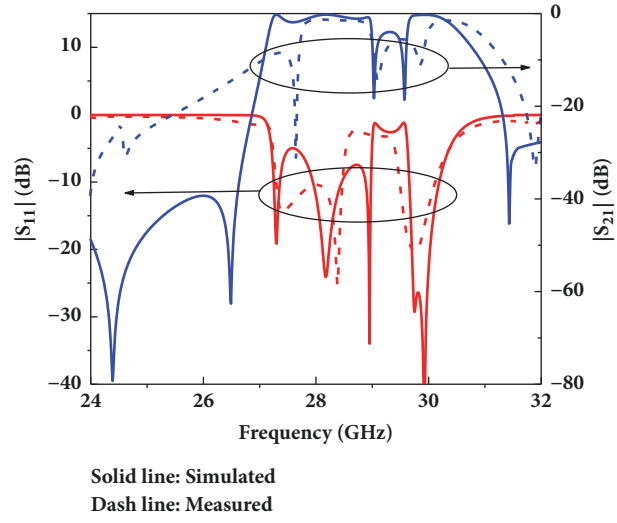

Figure 8: Simulated and measured results of the proposed dual-band BPF (solid line: simulated results; dash line: measured results).

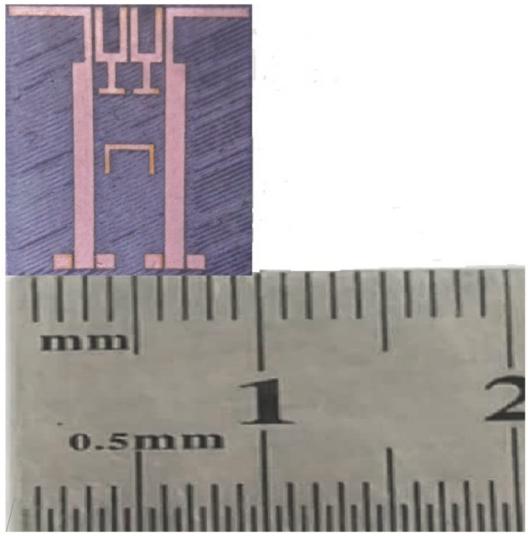

Figure 7: Photographs of this fabricated filter.

pair of I/O feedlines is W_1 =1.5 mm. A photograph of the proposed filter is shown in Figure 7. The filter size is 8×9 mm^2 (1.17λg X 1.04λg, where λg is the waveguide length at 28 GHz).

The measured and simulated results are shown in Figure 8, where the measured result is carried out by a Keysight N5227A network analyzer and Cascade probe station Summit 11K. A good agreement between simulation and measurement results is obtained. Two passbands are centred near 28.1 GHz and 31.1 GHz, with -3 dB fractional bandwidths (FBWs) of 6.4% and 3.8%, respectively. There are five transmission zeros on both sides of the passband, which greatly improve the filter's selectivity. The attenuation slope of the first passband generated at 28.1 GHz is 271 dB/GHz on the left side and 38.25 dB/GHz on the right side; the attenuation slope of each side of the second passband generated is 70.323 dB/GHz and 30.04 dB/GHz, respectively. A little higher insertion loss in the passband and frequency shift can be observed. The deviations between the simulated and measured results are mainly caused by two reasons. One is due to fabrication tolerance; millimetre-wave filters are very sensitive to their fabrication precision. Second, the discontinuity between the RF probe and our filter is not considered in our simulation, which may not be ignored at high frequencies.

To further demonstrate the performance of the proposed dual-band filter, comparisons with previously reported millimetre filters are listed in Table 1. It can be found that the proposed filter has achieved a very good trade-off between selectivity, size, and fabrication cost.

5. Conclusion

A highly selective planer millimetre-wave dual-band BPF is developed by cascading two dual-mode open-loop resonators with a pair of L-shaped feedlines. Two odd modes resonate at the lower passband and two even modes work at the higher passband. The proposed U-shaped nonresonating node is used to generate cross coupling. As a result, five transmission zeros are obtained, which effectively enhances this filter's selectivity. Finally, a millimetre-wave dual-band BPF is fabricated with a measured centre frequency of 28.1 GHz and 31.1 GHz and an FBW of 6.4% and 3.8%, respectively. This design achieves a very good trade-off between performance and fabrication cost.

Data Availability

The data used to support the findings of this study are available from the corresponding author upon request.

Conflicts of Interest

The authors declare that there are no conflicts of interest regarding the publication of this paper.

Acknowledgments

This work is partly supported by the National Science and Technology Major Project of the Ministry of Science and Technology of China (under Grant no. 2016ZX03001007) and partly supported by the National Natural Science Foundation of China (under Grant no. 61370008).

References

[1] *Third Generation Partnership Project (3GPP) Release 16*, http://www.3gpp.org/release-16.

[2] J. R. Garai, J. A. Cruz, J. M. Rebollar, and T. Estrada, "In-line pure E-plane waveguide band-stop filter with wide spurious-free response," *IEEE Microwave and Wireless Components Letters*, vol. 21, no. 4, pp. 209–211, 2009.

[3] K. Gong, W. Hong, Y. Zhang, P. Chen, and C. J. You, "Substrate integrated waveguide quasi-elliptic filters with controllable electric and magnetic mixed coupling," *IEEE Transactions on Microwave Theory and Techniques*, vol. 60, no. 10, pp. 3071–3078, 2012.

[4] F. Zhu, W. Hong, J.-X. Chen, and K. Wu, "Cross-coupled substrate integrated waveguide filters with improved stopband performance," *IEEE Microwave and Wireless Components Letters*, vol. 22, no. 12, pp. 633–635, 2012.

[5] S. O. Nassar and P. Meyer, "Pedestal substrate integrated waveguide resonators and filters," *IET Microwaves, Antennas & Propagation*, vol. 11, no. 6, pp. 804–810, 2017.

[6] T.-M. Shen, T.-Y. Huang, C.-F. Chen, and R.-B. Wu, "A laminated waveguide magic-T with bandpass filter response in multilayer LTCC," *IEEE Transactions on Microwave Theory and Techniques*, vol. 59, no. 3, pp. 584–592, 2011.

[7] A.-L. Franc, E. Pistono, D. Gloria, and P. Ferrari, "High-performance shielded coplanar waveguides for the design of CMOS 60-GHz bandpass filters," *IEEE Transactions on Electron Devices*, vol. 59, no. 5, pp. 1219–1226, 2012.

[8] Y. Zhong, Y. Yang, X. Zhu, E. Dutkiewicz, K. M. Shum, and Q. Xue, "An On-Chip Bandpass Filter Using a Broadside-Coupled Meander Line Resonator with a Defected-Ground Structure," *IEEE Electron Device Letters*, vol. 38, no. 5, pp. 626–629, 2017.

[9] S. Chakraborty, Y. Yang, X. Zhu et al., "A broadside-coupled meander-line resonator in 0.13-μm SiGe technology for millimeter-wave application," *IEEE Electron Device Letters*, vol. 37, no. 3, pp. 329–332, 2016.

[10] M. Sanchez-Renedo and R. Gomez-García, "Multi-coupled-resonator dual-band bandpass microstrip filters with non-resonating nodes," in *Proceedings of the 2011 IEEE/MTT-S International Microwave Symposium - MTT 2011*, pp. 1–4, Baltimore, MD, USA, June 2011.

[11] P.-J. Zhang and M.-Q. Li, "Cascaded trisection substrate-integrated waveguide filter with high selectivity," *IEEE Electronics Letters*, vol. 50, no. 23, pp. 1717–1719, 2014.

[12] Z. He, C. J. You, S. Leng, and X. Li, "Compact inline substrate integrated waveguide filter with enhanced selectivity using new non-resonating node," *IEEE Electronics Letters*, vol. 52, no. 21, pp. 1778–1780, 2016.

[13] D. Rebenaque, F. Pereira, J. Gomez Tornero, J. Garcia, and A. Alvarez Melcon, "Two simple implementations of transversal filters with coupling between non-resonant nodes," in *Proceedings of the IEEE MTT-S International Microwave Symposium Digest, 2005.*, pp. 957–960, Long Beach, CA, USA.

[14] S. Cogollos, R. Cameron, R. Mansour, M. Yu, and V. Boria, "Synthesis and Design Procedure for High Performance Waveguide Filters Based on Nonresonating Nodes," in *Proceedings of the 2007 IEEE/MTT-S International Microwave Symposium*, pp. 1297–1300, Honolulu, HI, USA, June 2007.

[15] J.-S. Hong, H. Shaman, and Y.-H. Chun, "Dual-mode microstrip open-loop resonators and filters," *IEEE Transactions on Microwave Theory and Techniques*, vol. 55, no. 8, pp. 1764–1770, 2007.

[16] X. Guan, Y. Yuan, L. Song et al., "A novel triple-mode bandpass filter based on a dual-mode defected ground structure resonator and a microstrip resonator," *International Journal of Antennas and Propagation*, vol. 2013, 2013.

[17] Chia-Mao Chen, Shoou-Jinn Chang, Sung-Mao Wu, Yuan-Tai Hsieh, and Cheng-Fu Yang, "Investigation of Compact Balun-Bandpass Filter Using Folded Open-Loop Ring Resonators and Microstrip Lines," *Mathematical Problems in Engineering*, vol. 2014, Article ID 679538, 6 pages, 2014.

[18] D. Zhang, J. Zhou, and Z. Yu, "Coupling topology of substrate integrated waveguide filter using unequal length slots with non-resonating nodes," *IEEE Electronics Letters*, vol. 53, no. 20, pp. 1368–1370, 2017.

[19] S. Amari and G. Macchiarella, "Synthesis of inline filters with arbitrarily placed attenuation poles by using nonresonating nodes," *IEEE Transactions on Microwave Theory and Techniques*, vol. 53, no. 10, pp. 3075–3081, 2005.

[20] S. Amari, "Direct synthesis of cascaded singlets and triplets by non-resonating node suppression," in *Proceedings of the 2006 IEEE MTT-S International Microwave Symposium Digest*, pp. 123–126, USA, June 2006.